Liquid–Gas Interfacial Plasmas for the Formation of Novel Nanobiomaterials*)

Toshiro KANEKO[1,2)], Kazuhiko BABA[1)] and Rikizo HATAKEYAMA[1)]

[1)]*Department of Electronic Engineering, Tohoku University, Sendai 980-8579, Japan*

[2)]*CREST/JST, Tokyo 102-0075, Japan*

(Received 4 December 2008 / Accepted 3 April 2009)

The liquid–gas interfacial region, which is the boundary between plasmas and liquids, activates physical and chemical reactions, thus attracting much attention as a novel reactive field in nanobiomaterial creation. Owing to the unique properties of ionic liquids such as their extremely low vapor pressure and high heat capacity, we successfully created a reactive liquid–gas (ionic liquids–plasmas) interfacial field under a low gas pressure condition, in which the plasma ion behavior can be controlled. The effects of plasma ion irradiation on the liquid medium are for the first time revealed quantitatively. In connection with the plasma ion irradiation, the potential structure and optical emission properties of the liquid–gas interfacial plasma were investigated by changing the polarity of the electrode in the liquid to evaluate liquid–plasma interactions. These results may contribute to systematizing the field of liquid–gas interfacial plasma physics for certain applications. Furthermore, novel nanobiocomposite materials, such as DNA-encapsulated carbon nanotubes, were formed using liquid-phase plasma, and for the first time, modifications of the electrical properties of nanocarbons according to the types of encapsulated DNA were demonstrated.

Keywords: liquid–gas interfacial plasma, ionic liquid, ion irradiation, potential structure, nanobiomaterial

DOI: 10.1585/pfr.4.028

1. Introduction

Pioneering liquid-phase plasma studies were conducted by Gubkin in 1887 [1]. In the middle of the 20th century, Hickling [2], Kanzaki [3], and Cserfalvi [4] performed systematic fundamental studies into liquid-phase plasmas, and Locke [5] investigated various types of liquid-phase plasmas for several environmental applications, such as wastewater treatment. Furthermore, recent advances in the generation of plasmas using arc [6], streamer [7, 8], pulsed direct current (DC) glow [9], and microwave [10, 11] discharges in liquids such as water, organic solvent [12], and supercritical carbon dioxide [13] have pioneered new fields relating to not only wastewater treatment but also sterilization, the microanalysis of liquid ingredients, and nanomaterial creation based on their distinctive properties such as their ultra high density, high reactivity, and high process rate. In these cases, the discharge is sustained in gas bubbles generated in the liquid, and therefore, it has been recognized that an understanding of the interfacial surface of the bubbles as a plasma-generation space in liquid is key to making the best use of liquid-phase plasmas as a reaction field. However, it is difficult to analyze the properties in the interfacial region of the bubbles, because of their dynamical behavior in liquid, and as a result, the precise structure of the interface between liquid and bubbles (gas or plasma) remains an open question. In this sense, the generation of a static liquid–gas interface is necessary to clarify phenomena at the interface as part of fundamental research on liquid-phase plasmas.

In this study, we developed a new plasma system to create a spatially and temporally stable liquid–plasma interfacial surface [14–16], i.e., a discharge plasma is generated just above the liquid by applying power to an electrode immersed in the liquid against a grounded electrode set in the gas-phase region. Here, the precise potential structure between these electrodes through the liquid–gas interfacial region is clarified for the first time, and the dynamics of the plasma ions can be controlled using the sheath electric field in the interfacial region. Control of the plasma irradiation flux and energy to the liquid leads to the creation of various types of nanoparticles [9, 17, 18] and means that particle size can be controlled.

Furthermore, we can create novel nanocarbons encapsulating a biomolecule such as DNA [19] using a liquid plasma called "electrolyte plasma" [20], and can demonstrate, for the first time, modifications of the electrical properties of nanocarbons according to the types of encapsulated DNA.

author's e-mail: kaneko@ecei.tohoku.ac.jp

*) This article is based on the invited talk at the 14th International Congress on Plasma Physics (ICPP 2008).

2. Liquid–Gas Interfacial Plasmas

2.1 Ionic liquids

To form stable plasma contacting with liquid, we adopt ionic liquids [21, 22], which have recently received much attention in the field of electrochemistry. Ionic liquids have some interesting characteristics, such as they consist of only positive and negative ions, i.e., no neutral solvent, have extremely low vapor pressure, high heat capacity, and are nonflammable. These characteristics enable us to introduce ionic liquids to a vacuum system and discharge plasma. Therefore, ionic liquids are the most suitable type of liquid for the formation of nanocomposite materials using discharge plasmas in contact with liquids.

2.2 Experimental apparatus

Figure 1 shows schematic diagrams of the experimental setup of a glass cell with a 15 mm inner diameter and measuring 10 mm deep in a cylindrical glass chamber 75 mm in diameter and 200 mm long. A powered electrode composed of a platinum plate 15 mm in diameter is located inside the glass cell, and an ionic liquid is introduced on the powered electrode. DC power is supplied to the powered electrode in the ionic liquid. On the other hand, a grounded electrode composed of a stainless steel (SUS) plate is set in the gas-phase region at a distance of 70 mm from the powered electrode. This discharge configuration is defined as "A-mode" and is shown in Fig. 1 (a).

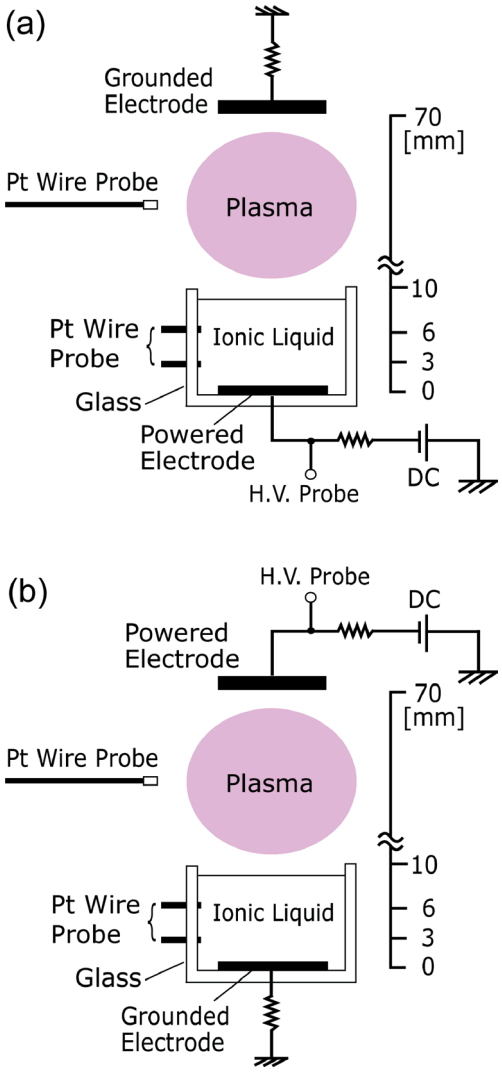

Fig. 1 Schematic diagrams of the experimental setup for DC discharge plasmas in contact with ionic liquid in (a) A-mode and (b) B-mode.

To examine the effects of the DC power supplied to the electrode in the ionic liquid on discharge-related phenomena, the powered electrode is switched to the SUS plate in the gas phase, and the platinum electrode in the ionic liquid is grounded instead, defined as "B-mode" and shown in Fig. 1 (b). Argon gas is adopted as a discharge medium, and the gas pressure P_{Ar} is varied from approximately 40 Pa to 80 Pa.

A type of ionic liquid (1.5 ml), 1-buthl-3-methylimidazolium tetrafluoroborate ($BMI^+BF_4^-$), is introduced into the glass cell. A high-voltage probe is connected directly to the powered electrode to measure its bias voltage. A Langmuir probe is inserted at the position of z = 20-60 mm to measure the parameters of the plasma in contact with the ionic liquid (z = 0; surface of electrode in the ionic liquid). The potential in the ionic liquid can also be measured using electrostatic probes (z = 3 mm and 6 mm).

2.3 Experimental results

We successfully generated ionic liquid-incorporated plasmas at low gas pressures with high stability, similar to normal glow discharge plasmas. Figure 2 shows an image of the DC discharge plasma on the ionic liquid in A-mode for P_{Ar} = 60 Pa, discharge voltage $V_D \sim -270$ V, and discharge current I_D = 1 mA. It was found that the static interfacial region between the plasma and the ionic liquid was generated stably.

Figure 3 presents axial profiles of the space potential

Fig. 2 Image of the stable DC discharge plasma on the ionic liquid in A-mode.

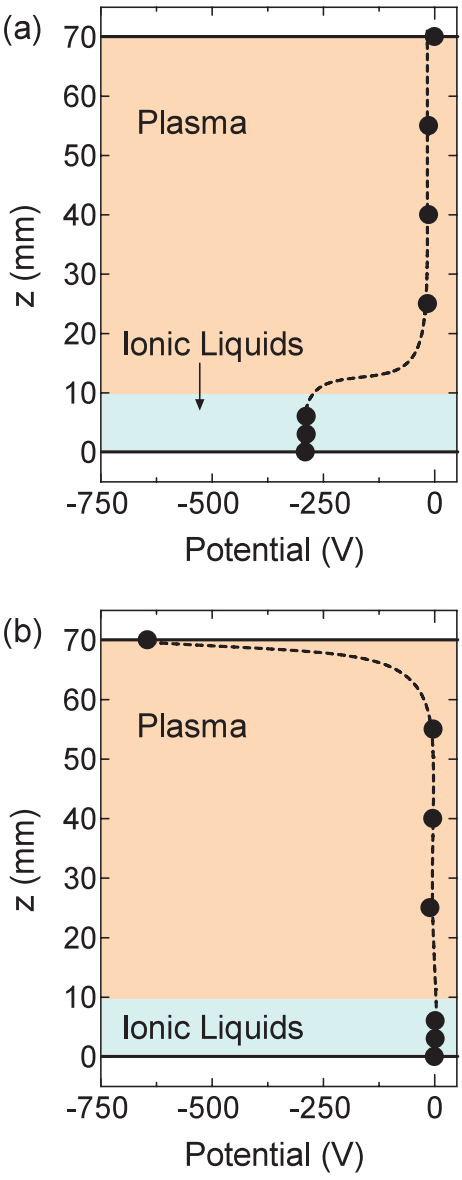

Fig. 3 Axial potential profiles estimated from the measurement of space potential in the plasma region and the floating potential in the ionic liquid for (a) A-mode and (b) B-mode. P_{Ar} = 30 Pa and I_D = 1 mA.

in the plasma region and the floating potential in the ionic liquid for (a) A- and (b) B-modes in the case of P_{Ar} = 30 Pa and I_D = 1 mA. The discharge voltage, i.e., the potential of the powered electrode, is about −290 V in the presence of ionic liquid in A-mode, and the potential in the ionic liquid is almost the same as that of the powered electrode in the ionic liquid. On the other hand, the potential in the plasma region is ∼5 V, which is lower than that of the grounded electrode, because the electrons that lost their energy through collision are accelerated in the region just below the grounded electrode that serves as an anode, called the "anode glow region," in order to sustain the discharge. Therefore, the potential difference between the plasma and the ionic liquid is about 285 V, and a sheath electric field is formed on the ionic liquid, giving rise to the electrostatic acceleration of positive ions from the plasma, i.e., ion irradiation, to the ionic liquid.

In B-mode, however, the potential in the ionic liquid is 0 V because the electrode in the ionic liquid is grounded. As the potential in the plasma region is about −5 V, the potential difference between the plasma and the ionic liquid is very small (∼5 V) and the electric field direction is opposite to that in A-mode. Therefore, instead of the positive ion irradiation, the electrons in the plasma shower to the ionic liquid. Furthermore, the discharge voltage in B-mode is −650 V, which is much larger than that in A-mode. This indicates that the ionic liquid works as the powered electrode in A-mode, and secondary electrons are emitted from the ionic liquid more efficiently than from the SUS electrode in B-mode, because the discharge voltage is dependent on the number of secondary electrons from the powered electrode.

The decrease in the breakdown voltage is also considered to be attributed to the concentration of the electric field on the ionic liquid surface, which is reported to have a string-shaped alkyl chain aligned along the electric field toward the gas-phase region [23].

Figure 4 shows the colors of the ionic liquid after the discharge, together with ultraviolet-visible (UV-vis) absorption spectra, in the cases of (a) A- and (b) B-modes, where P_{Ar} = 60 Pa and I_D = 1 mA. In A-mode, the color of the ionic liquid is observed to change gradually to deep yellow with time and the spectrum peak around 300 nm gradually increases. The stable plasma is maintained even after the color of the ionic liquid becomes deep yellow. In B-mode, on the other hand, the color of the ionic liquid remains clear and colorless, and the UV-vis spectra are also unchanged. This means that the change in color does not result from ultraviolet rays radiated from the plasma.

Based on these results, it is concluded that the molecular structure of the ionic liquid changes as a result of the high-energy ion irradiation when the powered electrode is in the ionic liquid (A-mode), because the positive ions in the gas-phase plasma are strongly accelerated by the sheath electric field formed on the ionic liquid.

Figure 5 shows optical emission spectroscopy (OES) spectra in the gas-phase plasma region, which indicate whether the species in the plasma is changed by the ion irradiation to the ionic liquid. The spectrum peak at 390 nm, which corresponds to a methylidyne radical (CH), is observed only in A-mode (Fig. 5 (a)). The intensity of the CH peak is plotted as a function of time, as shown in Fig. 6, and it is found that the CH peak intensity increases gradually with time only in A-mode and saturates at around 20 s. These phenomena can be explained by the fact that the high-energy ion irradiation causes the dissociation of the alkyl chain of the ionic liquid, and the dissociated CH is transported to the gas-phase plasma region from the ionic liquid region. In these OES spectra, we can find OH (308 nm) and H_α (656 nm) peaks in both A- and B-modes.

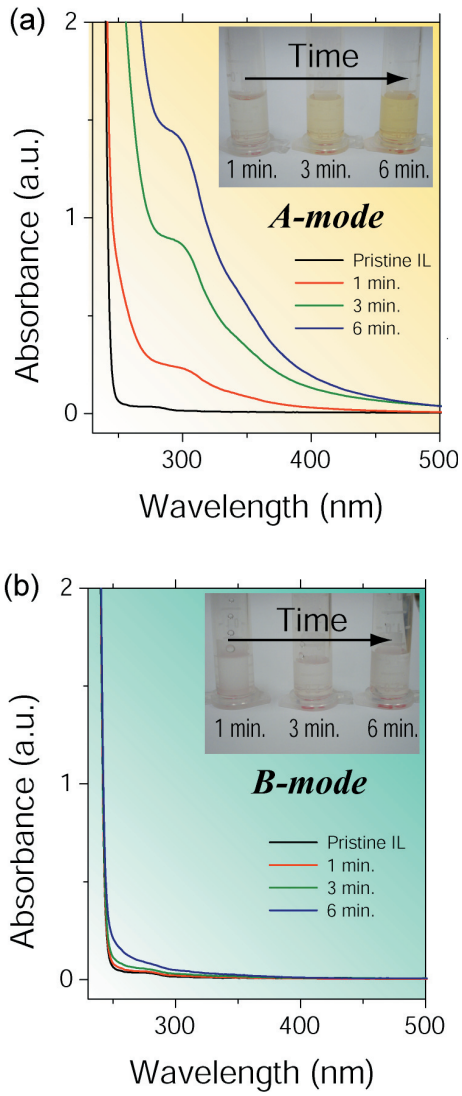

Fig. 4 Images of ionic liquid colors together with ultraviolet-visible absorption spectra as a function of discharge time in (a) A-mode and (b) B-mode for P_{Ar} = 60 Pa and I_D = 1 mA.

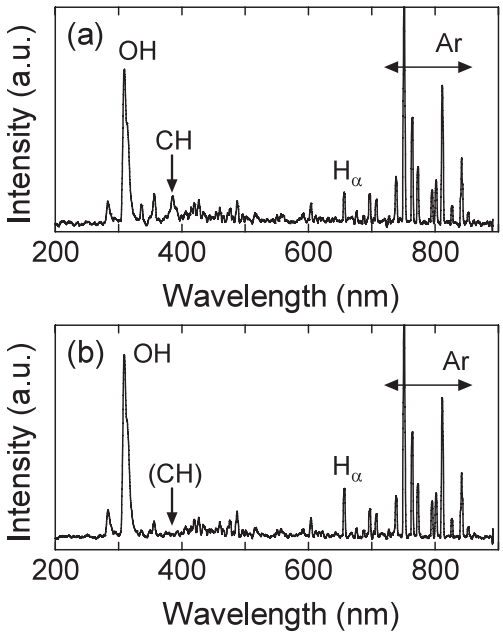

Fig. 5 Optical emission spectra in the gas plasma region in (a) A-mode and (b) B-mode.

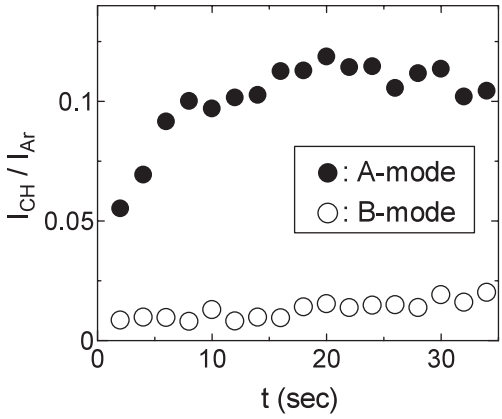

Fig. 6 Temporal evolution of the spectrum peak intensity of CH (390 nm) normalized by that of Ar (751 nm).

These peaks result from the very small amount of water present in the ionic liquid as an impurity, which is evaporated and dissociated in the gas plasma not only in A-mode but also in B-mode. This phenomenon is evidence that the CH peak observed only in A-mode is caused by the ion irradiation. Here, we emphasize that it is possible that this ion irradiation to the ionic liquid causes an effective reaction for material synthesis at the liquid–gas interface.

Using this ion irradiation, we attempted to synthesize gold nanoparticles in the ionic liquid by reduction of an Au compound, such as $HAuCl_4 \cdot 3H_2O$ [9]. Here, we use both A- and B-modes, which cause the ion irradiation and electron shower, respectively. In both these cases, Au nanoparticles can be formed, which is confirmed by transmission electron microscopy (TEM) and energy dispersive X-ray analysis (EDX). It should be noted that the efficiency of the synthesis of Au nanoparticles differs between the methods of ion irradiation and electron shower.

Figure 7 shows photos of the ionic liquid after 1-minute plasma irradiation in (a) A- and (b) B-modes. In the case of B-mode, only a slight change in color was observed compared with that without the plasma irradiation. In A-mode, however, it was found that the black material floated in the liquid–gas interfacial region, indicated by the red circle in Fig. 7 (a). The black material was confirmed to be Au nanoparticles. The reduction reaction of the Au ions is considered to be caused by the hydrogen radical H*, which is generated from the dissociation from the ionic liquid. Based on these results, we can conclude that compared with electrons, the hydrogen radical is more effective in the reduction of Au ions, and efficient Au nanoparticle synthe-

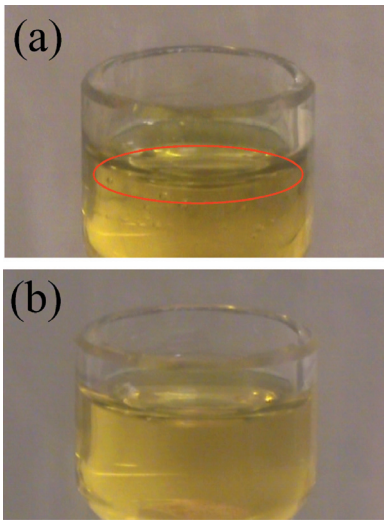

Fig. 7 Images of the ionic liquid in the glass cell after plasma irradiation for 1 min in (a) A-mode and (b) B-mode. The red circle indicates the black materials floating in the liquid–gas interfacial region in A-mode.

sis is realized by using the ion irradiation in the liquid–gas interfaced plasmas.

3. Electrolyte Plasmas

3.1 DNA electrolyte plasmas

We direct our attention to biomolecules, e.g., DNA, as a functional material encapsulated into single-walled carbon nanotubes (SWNTs). We choose DNA because it consists of four types of base, each of which has a different electronic property [24, 25], and the electronic properties on the nanoscale can be controlled by selecting the base sequence of DNA. In addition, because the structural weakness of DNA molecules would be protected by the surrounding SWNT wall, they have the potential to be applied to electronic devices, which could also be used for biomedical applications. As DNA is stable and forms negative ions easily in solution, we applied the ion irradiation method [26] to the electrolyte solutions with DNA mainly consisting of negative (DNA^-) and positive (hydrogen H^+) ions and neutral particles (H_2O), which can consequently be regarded as "electrolyte plasmas."

The basic behavior of ions in electrolyte plasmas can be understood using Debye and Huckel's theory [27], the scheme of which is almost the same as that with the gas-phase plasmas. The plasma parameters of the gas and electrolyte plasmas are compared and shown in Table 1. T, n, λ_D, and Γ denote electron (ion) temperature, electron (ion) density, Debye length, and the coupling coefficient, respectively. Both the gas and electrolyte plasmas consist of ions and neutral particles and are electrically quasineutral. Thus, the behavior of the ions in electrolyte plasmas is predicted to be the same as that in gas plasmas.

Debye lengths in the gas and electrolyte plasmas are represented by Eqs. (1) and (2), respectively, where k_B, N_A, ε_0, ε_r, I, c, z, and j are the Boltzmann constant, Avogadro's number, permittivity in vacuum, specific permittivity, ionic strength, concentration of electrolyte, valence of ions, and ion species in the electrolyte plasmas, respectively. Because the ionic strength I includes the concentration of the electrolyte c and the valence of ions, the $N_A I$ term in Eq. (2) is generally much larger than the n term in Eq. (1) when a polyelectrolyte in the electrolyte plasmas, such as multivalent DNA, is adopted. As a result, the Debye length in the electrolyte plasmas is five orders of length shorter than that in the conventional gas plasmas, which causes an extremely strong electric field, i.e., a sheath electric field in front of the electrodes immersed in the electrolyte plasmas. On the other hand, the coupling coefficient Γ, defined by Eq. (3), is around 2.5 in the case of the electrolyte plasmas, where d is the average distance between ions. Because Γ is the ratio of the nearest-neighbor Coulomb energy to the thermal energy of particles and Γ in the liquid phase is generally distributed in the range from 1 to 100, $\Gamma \sim 2.5$ is a reasonable value for solutions for electrolyte plasmas.

$$\lambda_D = \left(\frac{\varepsilon_0 k_B T}{ne^2}\right)^{1/2}, \tag{1}$$

$$\lambda_D = \left(\frac{\varepsilon_0 \varepsilon_r k_B T}{2N_A I e^2}\right)^{1/2}, \quad I = \frac{1}{2}\sum_j c_j z_j^2, \tag{2}$$

$$\Gamma = \frac{e^2 Z_j^2 / 4\pi\varepsilon_0 d}{k_B T}. \tag{3}$$

Since the electrolyte plasmas are in the liquid phase, the ion temperature is quite low compared with that in the gas plasmas. The ion density in the electrolyte plasmas is essentially much higher than that in the gas plasmas under our typical conditions, which is significantly useful in terms of rapid reaction for material creation.

In the case of the electrolyte plasmas, however, relatively strong electric fields are required to control the ion irradiation, because the large amounts of neutral particles obstruct ion motion through ion–neutral collisions. Therefore, any gap between electrodes, to which voltages are applied in the ion irradiation method, should be small in order to induce strong electric fields in the electrolyte plasmas. In this section, we elaborate on the formation of DNA-encapsulated SWNTs using the plasma ion irradiation method in the electrolyte plasmas.

3.2 Experimental apparatus

Figure 8 presents a schematic of the experimental apparatus for DNA negative-ion irradiation in the DNA electrolyte plasma, where the DNA molecule is dissolved in pure water. DC and/or radio frequency (RF) electric fields are applied independently to the DNA electrolyte plasma by supplying DC (V_{DC}) and/or RF (V_{RF}) voltages to aluminum (Al) electrodes (anode and cathode) immersed in the electrolyte plasma. When only the DC electric field

Table 1 Comparison of parameters between gas and electrolyte plasmas.

	Gas plasmas [a]	Electrolyte plasmas [b]
Components	electrons, positive ions, neutral particles	positive and negative ions, neutral particles
Charge	quasineutral	quasineutral
T	~3.0 eV	0.025 eV (300 K)
n	$\sim 10^{10}$ cm^{-3}	$\sim 10^{15}$ cm^{-3}
λ_D	~0.13 mm	~11 nm
Γ	$\ll 1$	~2.5

[a] Typical direct current discharge plasma.
[b] Concentration of DNA (A_{15}) is assumed to be 7×10^{-6} mol/l.

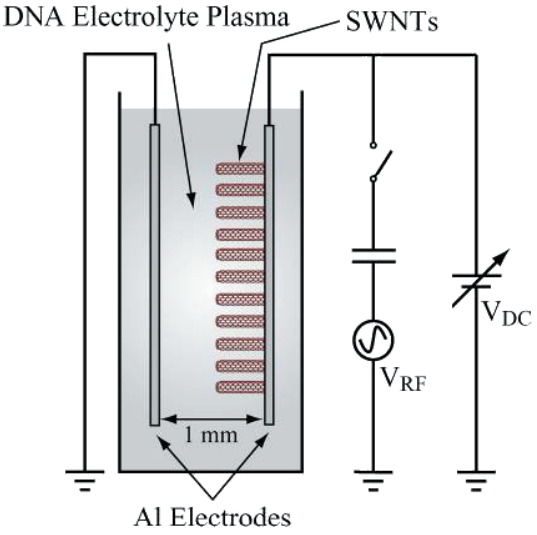

Fig. 8 Schematic of the experimental setup for DNA irradiation in electrolyte plasma. Both the DC and RF electric fields are superimposed upon an Al electrode, which is covered with SWNTs.

is applied, the DNA molecule is considered to be irradiated to the anode similar to electrophoresis because of the negative charge of the DNA molecule. In this situation, the DNA molecule assumes a random-coil conformation through the Brownian motion in the solution. When only the RF electric field is applied, however, a dominant dipole moment is induced along the DNA axis because of its high anisotropy, resulting in stretching of the DNA molecule parallel to the external electric field owing to the interaction between the external field and the induced dipole [28]. In addition, a type of ponderomotive force (dielectrophoresis) [29] generated by the spatial gradient of the RF electric field is theoretically believed to influence the movement of the stretched and orientated DNA molecule toward both the electrodes. If both the DC and the RF electric fields are applied simultaneously to the DNA electrolyte plasma, the respective effects, i.e., irradiation and stretching, are superimposed.

SWNTs are treated by heat in order to open their tips in advance. Open-ended SWNTs are coated onto the aluminum anode, which is submerged in the DNA electrolyte plasma. The distance between the anode and cathode is 1 mm, and the volume of the electrolyte plasma is 5 cm^3.

The DNA negative ions are adsorbed onto the anode aluminum surface after irradiating the electrode, and the adsorption is maintained semipermanently [28]. Therefore, the amount of DNA negative ions irradiated to the anode can be estimated by measuring the absorbance of the DNA solution after applying the DC and/or RF electric fields [19]. In this experiment, several types of single-stranded DNA are used. The notation of DNA is as follows. The bases of adenine, thymine, guanine, and cytosine are represented by A, T, G, and C, respectively. In addition, the number of bases is denoted by subscripts; for example, a DNA molecule consisting of 15 adenines is represented by A_{15}.

3.3 Experimental results

After the irradiation of DNA to the anode, the SWNTs on the electrode are sonicated for cleaning the surface of the excess DNA (adherence) and analyzed by Raman-scattering spectroscopy. Figure 9 presents Raman spectra of SWNTs in the region of the radial breathing mode (RBM). Because the RBM mode is the stretching mode of SWNTs in the radial direction, this mode is considered to be sensitive to the encapsulation of other materials in SWNTs. The spectrum shape changed in any case after the DNA negative-ion irradiation compared with that of pristine SWNTs, shown in particular by the drastic decrease in the peak intensity at 164 cm^{-1}. The changes observed in the peak intensity in the range of RBM are considered to be one set of phenomena associated with interactions between encapsulated DNA and SWNTs.

In order to investigate the effects of a base sequence on the encapsulation, different bases such as cytosine (C_{30}) and guanine/adenine (AG_{30}) were used for the same procedures, as shown in Fig. 9, where V_{DC} = 10 V and V_{RF} = 150 V. In this situation, the Raman spectrum of AG_{30} changes drastically compared with that of C_{30}. Figure 10 shows redox potentials (reduction and oxidation po-

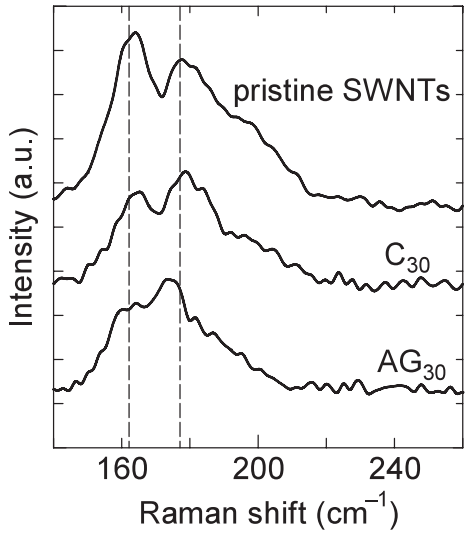

Fig. 9 Raman spectra of SWNTs after DNA irradiation with the base sequence as a parameter. The excitation wavelength of the laser is 488 nm. V_{DC} = 10 V and V_{RF} = 150 V.

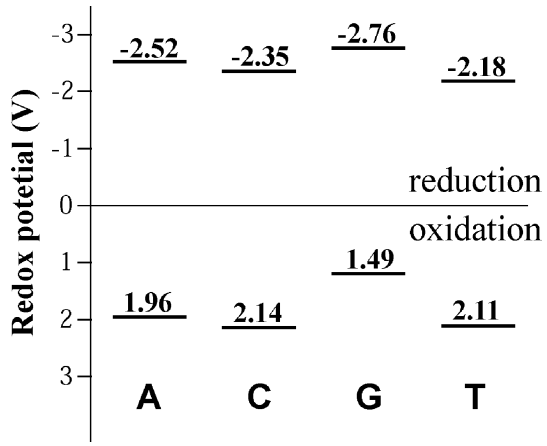

Fig. 10 Redox potentials of the four types of base. Guanine and cytosine have the lowest and highest oxidation potentials, respectively.

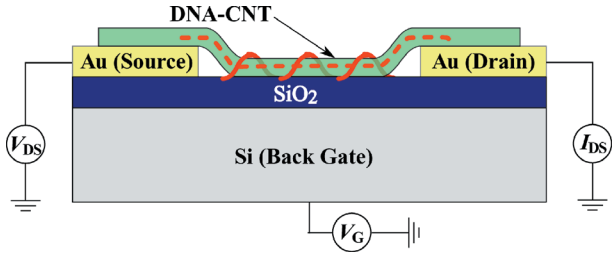

Fig. 11 Structure of DNA-irradiated carbon nanotube-based field effect transistor.

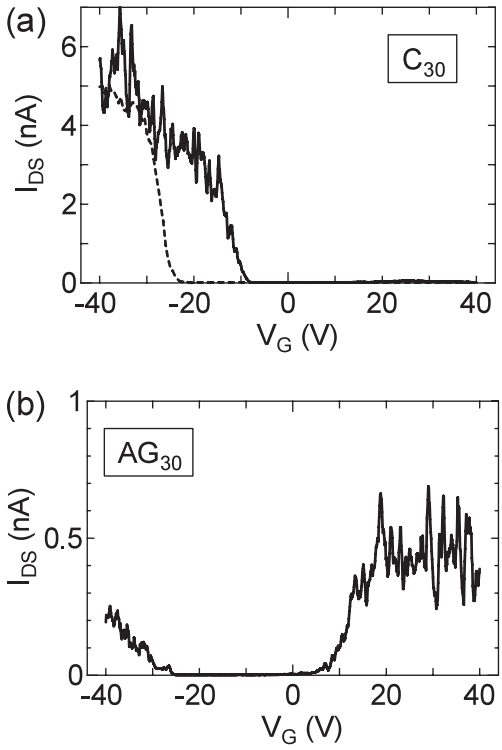

Fig. 12 Source-drain current (IDS) vs. gate voltage (VG) characteristics at room temperature for (a) pristine SWNT (dotted line) and C_{30}-irradiated SWNT (solid line), and (b) AG_{30}-irradiated SWNT. V_{DS} = 1 V.

tentials) of the four types of base [25], where guanine and cytosine have the lowest and highest oxidation potentials, respectively. Therefore, the change in the Raman spectrum of AG_{30}-encapsulated SWNTs is caused by the lowest oxidation potential (electron-donor-like property) of guanine, while the highest oxidation potential of cytosine has a relatively small effect on SWNTs. This means that the electronic modification of the SWNTs can be controlled by changing the base sequence of encapsulated DNA.

Using these electronically modified DNA irradiated SWNTs, we fabricated a SWNT-based FET (field effect transistor) device, as shown in Fig. 11. These SWNTs samples were ultrasonically dispersed in N, N-dimethylformamide first and then spincoated on FET substrates, each of which consisted of Au drain-source electrodes on a SiO_2 insulating layer. A heavily doped Si substrate served as a backgate. The detailed fabrication process for FET devices can be found elsewhere [30]. Electronic transport measurements, i.e., the drain-source current I_{DS} as a function of the gate voltage V_G for fixed drain-source voltage V_{DS}, were performed at room temperature under vacuum conditions on a semiconductor parameter analyzer (Agilent 4155C). The transport property of pristine semiconducting SWNTs is widely known to exhibit p-type behavior, which is shown as a dotted line in Fig. 12 (a), where a characteristic curve of I_{DS}–V_G is described for V_{DS} = 1 V. The transport property of the C_{30}-irradiated SWNTs is presented as a solid line in Fig. 12 (a). The typical p-type trait is observed, but the threshold voltage (V_{th}) for hole conductance is found to shift from −20 V

to −10 V compared with that of pristine SWNTs, indicating that the p-type behavior of the SWNTs is enhanced by the encapsulation of the C_{30}. In contrast, the transport property of the AG_{30}-irradiated SWNTs changes drastically to that of an n-type semiconductor (Fig. 12 (b)). This n-type behavior is attributed to the charge transfer between the guanine and local parts of the SWNTs.

Based on these results, the different types of base in DNA cause the modification of the electronic characteristics of the SWNT-based FET. Therefore, the formation of a p–n junction in SWNTs could be realized by encapsulating DNA as both the electron donor and the electron acceptor.

4. Conclusion

A DC discharge plasma was generated just above ionic liquid by applying DC voltage to an electrode immersed in the ionic liquid against a grounded electrode set in the gas-phase region. The precise potential structure between these electrodes through the liquid–gas interfacial region was clarified for the first time, and the dynamics of the plasma ions were found to be controllable using the sheath electric field in the interfacial region. Control of the plasma ion irradiation flux and energy to the ionic liquid leads to the creation of various types of nanoparticles and to controllable particle size. Furthermore, we have formed, for the first time, novel nanocarbons encapsulating DNA using electrolyte plasma and have demonstrated modifications to the electrical properties of the nanocarbons according to the type of irradiated DNA.

Acknowledgments

The author would like to thank Professor K. Tohji, Dr. T. Okada, Dr. Y.F. Li, and Mr. Y. Hirotsu for their collaboration.

This work was supported by a Grant-in-Aid for Scientific Research from the Ministry of Education, Culture, Sports, Science and Technology, Japan.

[1] J. Gubkin, Ann. Physik. **32**, 114 (1887).
[2] A.R. Denaro and A. Hickling, J. Electrochem. Soc. **105**, 265 (1958).
[3] Y. Kanzaki, M. Hirabe and O. Matsumoto, J. Electrochem. Soc. **133**, 2267 (1986).
[4] T. Cserfalvi and P. Mezei, J. Anal. At. Spectrom. **9**, 345 (1994).
[5] B.R. Locke, M. Sato, P. Sunka, M.R. Hoffmann and J.-S. Chang, Ind. Eng. Chem. Res. **45**, 882 (2006).
[6] N. Sano, H. Wang, M. Chhowalla, I. Alexandrou and G.A.J. Amaratunga, Nature (London) **414**, 506 (2001).
[7] I.V. Lisitsyn, H. Nomiyama, S. Katsuki and H. Akiyama, Rev. Sci. Instrum. **70**, 3457 (1999).
[8] K. Imasaka, J. Suehiro, Y. Kanatake, Y. Kato and M. Hara, Nanotechnol. **17**, 3421 (2006).
[9] J. Hieda, N. Saito and O. Takai, J. Vac. Sci. Technol. A **26**, 854 (2008).
[10] S. Nomura and H. Toyota, Appl. Phys. Lett. **83**, 4503 (2003).
[11] T. Ishijima, H. Hotta, H. Sugai and M. Sato, Appl. Phys. Lett. **91**, 121501 (2007).
[12] V.A. Ryzhkov, Physica B **323**, 324 (2002).
[13] T. Tomai, K. Katahira, H. Kubo, Y. Shimizu, T. Sasaki, N. Koshizaki and K. Terashima, J. Supercritical Fluids **41**, 404 (2007).
[14] K. Baba, T. Kaneko and R. Hatakeyama, Jpn. J. Appl. Phys. **45**, 8286 (2006).
[15] K. Baba, T. Okada, T. Kaneko, R. Hatakeyama and H. Yoshiki, Thin Solid Films **515**, 4308 (2007).
[16] K. Baba, T. Kaneko and R. Hatakeyama, Appl. Phys. Lett. **90**, 201501 (2007).
[17] S.A. Meiss, M. Rohnke, L. Kienle, S. Zein El Abedin, F. Endres and J. Janek, ChemPhysChem **8**, 50 (2007).
[18] T. Torimoto, K. Okazaki, T. Kiyama, K. Hirahara, N. Tanaka and S. Kuwabata, Appl. Phys. Lett. **89**, 243117 (2006).
[19] T. Okada, T. Kaneko, R. Hatakeyama and K. Tohji, Chem. Phys. Lett. **417**, 288 (2006).
[20] T. Kaneko, T. Okada and R. Hatakeyama, Contrib. Plasma Phys. **47**, 57 (2007).
[21] K.R. Seddon, Nature Mater. **2**, 363 (2003).
[22] R.D. Rogers and K.R. Seddon, Science **302**, 792 (2003).
[23] E. Sloutskin, B.M. Ocko, L. Tamam, I. Kuzmenko, T. Gog and M. Deutsch, J. Am. Chem. Soc. **127**, 7796 (2005).
[24] K.-H. Yoo, D.H. Ha, J.-O. Lee, J.W. Park, J. Kim, J.J. Kim, H.-Y. Lee, T. Kawai and H.-Y. Choi, Phys. Rev. Lett. **87**, 198102 (2001).
[25] D. Kato, N. Sekioka, A. Ueda, R. Kurita, S. Hirono, K. Suzuki and O. Niwa, J. Am. Chem. Soc. **130**, 3716 (2008).
[26] R. Hatakeyama, T. Hirata and G.-H. Jeong, Plasma Source Sci. Technol. **13**, 108 (2004).
[27] P. Debye and E. Huckel, Physikalische Zeitschrift **24**, 185 (1923).
[28] M. Washizu and O. Kurosawa, IEEE Trans. Ind. Appl. **26**, 1165 (1990).
[29] R. Krupke, F. Hennrich, H.B. Weber, M.M. Kappes and H.v. Lohneysen, Nano Lett. **3**, 1019 (2003).
[30] T. Izumida, R. Hatakeyama, Y. Neo, H. Mimura, K. Omote and Y. Kasama, Appl. Phys. Lett. **89**, 093121 (2006).